arXiv:1602.00082v1 [cond-mat.mes-hall] 30 Jan 2016

Strongly-coupled nanotube electromechanical resonators

Guang-Wei Deng,[1,2,*] Dong Zhu,[1,2,*] Xin-He Wang,[3,4,*] Chang-Ling Zou,[1,2,*] Jiang-Tao Wang,[3,4] Hai-Ou Li,[1,2] Gang Cao,[1,2] Di Liu,[1,2] Yan Li,[1,2] Ming Xiao,[1,2] Guang-Can Guo,[1,2] Kai-Li Jiang,[3,4] Xing-Can Dai,[3,4] and Guo-Ping Guo[1,2,†]

[1] *Key Laboratory of Quantum Information, University of Science and Technology of China, Chinese Academy of Sciences, Hefei 230026, China*

[2] *Synergetic Innovation Center of Quantum Information & Quantum Physics, University of Science and Technology of China, Hefei, Anhui 230026, China*

[3] *State Key Laboratory of Low-Dimensional Quantum Physics, Department of Physics & Tsinghua-Foxconn Nanotechnology Research Center, Tsinghua University, Beijing 100084, China*

[4] *Collaborative Innovation Center of Quantum Matter, Beijing 100084, China*

Coupling an electromechanical resonator with carbon-nanotube quantum dots is a significant method to control both the electronic charge and the spin quantum states. By exploiting a novel micro-transfer technique, we fabricate two strongly-coupled and electrically-tunable mechanical resonators on a single carbon nanotube for the first time. The frequency of the two resonators can be individually tuned by the bottom gates, and strong coupling is observed between the charge states and phonon modes of each resonator. Furthermore, the conductance of either resonator can be nonlocally modulated by the phonon modes in the other resonator. Strong coupling is observed between the phonon modes of the two resonators, which provides an effective long distance electron-electron interaction. The generation of phonon-mediated-spin entanglement is also analyzed for the two resonators. This strongly-coupled nanotube electromechanical resonator array provides an experimental platform for studying the coherent electron-phonon interaction, the phonon mediated long-distance electron interaction, and entanglement state generation.

I. INTRODUCTION

Carbon nanotubes (CNTs) [1] are noted for their nearly perfect structures with nanometer diameter, ultralow mass density, great mechanical strength and elastic properties, as well as ballistic electron transport [2, 3]. Owing to good electrical conductivity and lack of impurities and net nuclear spin, the electron charge and spin states in gate-defined CNT quantum dots (QDs) [4–8] are promising candidates for solid-state quantum information processing. However, a scalable quantum processor requires long-range couplings, which is a challenge for QDs, because there are only local interactions between neighboring QDs. Many researches have been undertaken on the development of a "quantum bus" to transfer quantum information, carried by electrons, over certain distances [9, 10]. For example, a single electron can be conveyed between QDs over distances of micrometers [11, 12], and an integrated superconducting microwave cavity can mediate the coupling between spins over distances of millimeters [9].

On the other hand, the excellent mechanical properties of CNTs enable their use as high frequency and high-quality-factor nanomechanical resonators [13, 14]. The vibrations of suspended CNTs can modulate the electrochemical potential of quantum dots, which leads to coherent coupling between single electron charge and phonon [15, 16]. Additionally, the deformation of CNTs can induce an effective transverse magnetic field applied on the electron spins that arises from the spin-orbit interaction [17–19], thereby allowing spin flips by phonons [20, 21]. These approaches provide avenues toward the coherent operation and transduction of the quantum state of CNT QDs by a phonon, or alternatively, the electronic manipulation of the phonon quantum state [22–27]. Theoretically, mechanically-induced two-qubit gates and maximally-entangled states for two spins trapped in a single CNT have recently been studied [28]. However, those previous works have only focused on the localized electron-phonon interactions. Hence, the great potential of using phonons as flying qubits for communicating electron spins over long-distance [29–31] is overlooked.

Here we demonstrate a highly-tunable electrically-coupled nanomechanical resonator system of a single CNT with two suspended sections. We developed a novel transfer method, which can precisely posit the CNT to the designated location and maintain the clean surface of the CNT without requiring of chemical treatment. In the conductance spectrum, an avoided crossing indicates a strong coupling between the two CNT electromechanical resonators and the hybridization of two modes, and also proves the strong coupling between the electron charge and individual hybrid mode. To our knowledge, this is the first demonstration of non-local coupling between an electron charge and phonon in a carbon nanotube. Our theoretical study also predicts that remote-entanglement

* These authors contributed equally to this work.
† Corresponding author: gpguo@ustc.edu.cn

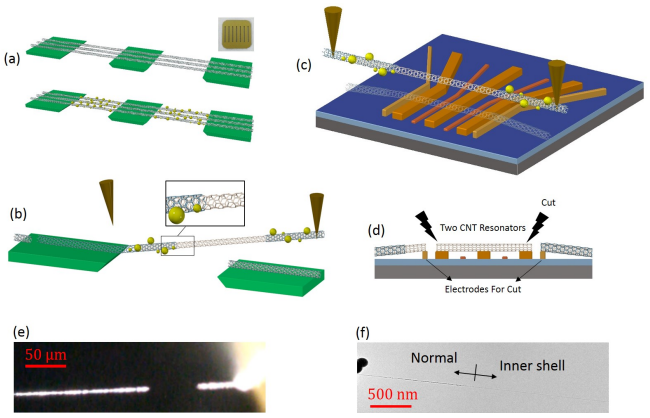

FIG. 1. **Transfer method** (a) Growth of the CNT using the ethane CVD method. The long, parallel CNTs are grown on a silicon substrate and suspended over trenches. Typically, the CNTs are double- or triple- walled. To obtain a direct visualization, we then deposit some TiO_2 nano-particles on the suspended parts of the CNTs. (b) With an optical microscope and two homemade tips, we cut and take off the outer shell of the suspended part of the CNT, maintaining the inner part, which is ultra clean. (c) After straining the individual CNT between the two tips, we place it onto the designed metal contacts, which have been biased with about 3-5 V for attracting the CNT. (d) Locally cutting off the redundant parts of the CNT. (e) Micrograph of the CNT, corresponding to Fig. 1(b), where the bright parts contain TiO_2 and the outer shell. The invisible part between the two bright parts only contains the inner shell. (f) Transmission electron micrograph of the CNT. Normal part corresponds to the bright parts in Fig. 1(e) and the inner shell corresponds to the invisible part.

spin-state preparation is feasible in this device, for practical experimental parameters.

II. RESULTS

A. Experiment Setup

Figure 1 shows the sample fabrication method, where a CNT (typically single- or double-walled, 2-3 nm in diameter and grown by chemical vapour deposition) is suspended over two trenches (1.2 μm wide, 200 nm deep) between three metal (Ti/Au) electrodes. The CNT is transferred by a novel near-field micro-manipulation method, by which the perfect clean single CNTs are deterministically and precisely posited on the electrodes, without degrading the quality of the CNT (see Fig. 1). The measurements are performed in a He3 refrigerator at a base temperature of approximately 270 mK and at pressures below 10^{-6} torr (see Methods for details).

The suspended CNT is biased and actuated by two electrodes underneath the CNT (Fig. 2(a)). Each suspended section of the CNT simultaneously serves as both a mechanical resonator and a quantum dot. The gate voltages, $V_{g1(2)}$, induce an average additional charge $\langle q_i \rangle = C_{gi}V_{gi}\,(i = 1, 2)$ on the CNT, where C_{gi} is the capacitance between the i-th gate and the CNT. The attraction between the charge q_i and its opposite charge $-q_i$ on the i-th gate causes an electrostatic force downward on the CNT, leading to a mean electrostatic force on the CNT as

$$F_i = \frac{\partial \langle U_i \rangle}{\partial z_i} = \frac{1}{2}\frac{\partial C_{gi}}{\partial z}(V_{gi}^{\rm DC} + \delta V_{gi})^2. \qquad (1)$$

Here, $\frac{\partial C_{gi}}{\partial z}$ is the derivative of the gate capacitance with respect to the distance between the gates and the CNT, while $V_{gi}^{\rm DC}$ and δV_{gi} are the DC bias and AC signal electric fields applied to the electrodes, respectively.

By applying a DC voltage $V_{gi}^{\rm DC}$, the nanobeam-type nanomechanical resonator can be deformed by the static force $F_i^{\rm DC} = \frac{1}{2}\frac{\partial C_{gi}}{\partial z}(V_{gi}^{\rm DC})^2$, and the induced additional tension on the CNT changes the frequencies of the mechanical resonances. In addition, the electron transport properties of the quantum dot also depend on the electrochemical potential on the dot, and so are controllable by the DC voltage. For instance, Figs. 2(b, c) show the currents $I_{1(2)}$ through the quantum dot as a function of gate voltage. The 1st quantum dot is working in the Coulomb blockade regime, while the 2nd is working in the Fabry-Perot interference regime [32]. Both quantum dots can be tuned to work in different regimes by changing the $V_{gi}^{\rm DC}$ [14, 33]. If an RF driving field $\delta V_{gi}(t) = \delta V_{gi}^{\rm RF}\cos(2\pi f_{gi}t)$ is applied, when the frequency f_{gi} approaches the resonance frequency $f_{0i} = \omega_{m,i}/2\pi$ of the i-th resonator, the periodic driving force $F_i^{\rm AC} = \frac{\partial C_{gi}}{\partial z}V_{gi}^{\rm DC}\delta V_{gi}(t)$ will effectively actuate the mechanical vibration. The phonons can also be generated by a parametric driving force $F_i^{\rm para} = \frac{1}{2}\frac{\partial C_{gi}}{\partial z}(\delta V_{gi}^{\rm RF})^2\cos^2(2\pi f_{gi}t)$ with $f_{gi} = f_{0i}/2$.

B. Individual nanotube resonators

Before studying the coupled resonators, we first investigate the two mechanical resonators independently. Owing to the RF driving force, we obtain the driving displacement vibration $\delta z(\omega, t) = A(\omega)\cos(\omega t + \phi)$, with driving frequency ω, amplitude of the mechanical oscillator

$$A(\omega) = \frac{\frac{\partial C_{gi}}{\partial z}V_{gi}^{\rm DC}\delta V_{gi}^{\rm RF}}{m_{\rm eff}} \times \frac{1}{\sqrt{(\omega_{m,i}^2 - \omega^2 + \frac{3}{4}\frac{\alpha}{m_{\rm eff}}A(\omega)^2)^2 + \frac{\omega_{m,i}^2\omega^2}{Q_i^2}}}, \qquad (2)$$

phase factor ϕ, effective mass $m_{\rm eff}$ and nonlinear Duffing term α. The displacement-modulated capacitor of the suspended CNT can modify the current, which has the same effect on the modulated gate voltage as $V_{{\rm eff,i}}(\omega, t) = \frac{V_{gi}^{\rm DC}}{C_{gi}}\frac{\partial C_{gi}}{\partial z}\delta z(\omega, t)$ [14, 34]. Therefore, the drain-source current changes with time as $I_{\rm SD,i}(t) =$

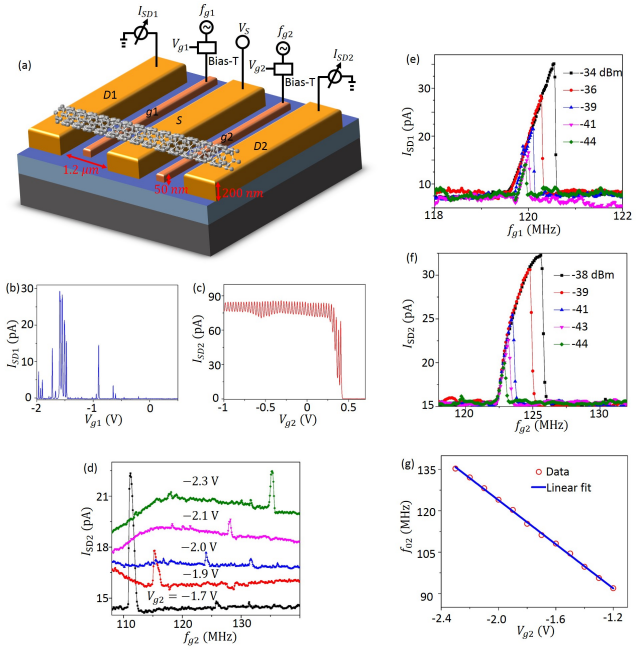

FIG. 2. **Measurement circuit and the mechanical vibrations modifying the current in the quantum dots.** (a) Schematic diagram of the coupled nanomechanical resonator and double quantum dot system. A single-walled carbon nanotube is transferred onto three 200 nm height Ti/Au electrodes, working as sources/drains. Thus, the three source/drain structure forms two coupled resonators in series. Two 50 nm Ti/Au electrodes are used as back gates to apply DC and AC voltages. (b-c) Electron transport properties of the two quantum dots. Both quantum dots are Coulomb blockaded at large positive gate voltages. Resonator 1 works like a quantum dot in the large-voltage range while resonator 2 works in the Fabry-Perot interference regime. Both resonators are biased at 5 mV.(d) Resonance current peaks of resonator 2 as a function of its driving frequency, for various gate voltages (noted in the figure). (e, f) The current spectrum versus driving frequency for various driving powers. (g) Resonance frequency of resonator 2 as a function of its gate voltage. The blue line is a linear fit, with an R-squared value of 99.9%.

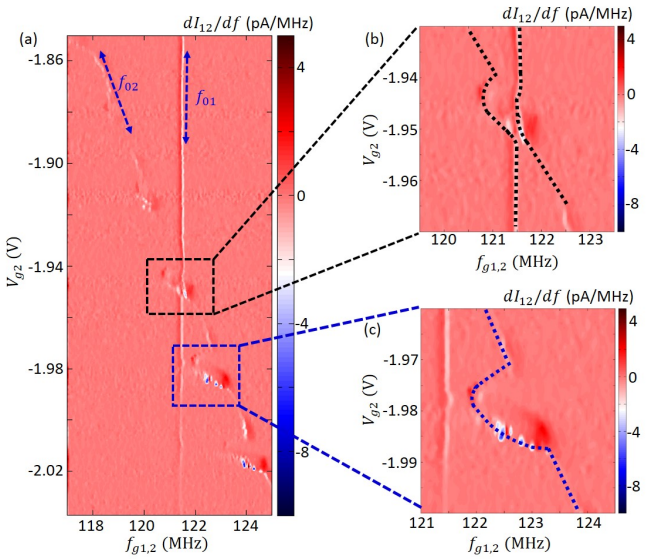

FIG. 3. **Strong electron-phonon coupling.** (a) Color map of the coupled system as a function of driving frequency and $V_{g2}^{\rm DC}$. $V_{g1}^{\rm DC}$ is fixed at −0.657 V, and the current I_{12} is measured between the D1 and D2 gates. The vertical line represents resonator 1, while the transverse lines correspond to the electron tunneling peaks of resonator 2. The oblique line with a negative slope represents the resonance of resonator 2. (b) Zoom-in of the crossing region for the two resonators and the current peak. (c) Zoom-in of the interaction between resonator 2 and its electron tunneling.

$\sum_n \frac{1}{n!}\frac{d^n I_{\rm SD,i}^{\rm DC}(V_{g,i})}{dV_{g,i}^n}[V_{\rm eff,i}(\omega,t)]^n$, with the $I_{\rm SD,i}^{\rm DC}$ shown in Fig. 2. The measured change of the DC current is approximated by

$$\Delta I_{sd,i} \approx \frac{1}{4}\frac{d^2 I_{\rm SD,i}^{\rm DC}(V_{g,i})}{dV_{g,i}^2}[\frac{V_{g,i}^{\rm DC}}{C_{g,i}}\frac{\partial C_{g,i}}{\partial z}A(\omega)]^2 \qquad (3)$$

to second order. Figure 2 shows the measured DC current as a function of driving frequency at low temperature, for various driving powers. For relatively low driving powers, the spectra show symmetry peaks. The Duffing coefficient α is measured to be of the order of $10^{12} kg/(m^2 s^2)$. High order nonlinearities begin to exist when the driving power is larger than -40 dBm. (see the supplementary materials).

The quality factor Q of the resonator and resonance frequency of the CNT resonator are determined by fitting the spectrum obtained at low driving power with a Lorentzian function. The quality factors of both resonators are $\sim 10^4$ (largest value in our measurements), which yield an energy relaxation time of 13 μs. Figs. 2(d, g) show the broadband tunability of the resonance frequency $f_{02} = \omega_{m,2}/2\pi$, which is linearly increased with $V_{g2}^{\rm DC}$. This can be explained as an incremental increase of the elastic tension on the nanotube, which is almost linearly proportional to the perturbative DC voltage applied to the gate. From the data for resonator 2, we fit the coefficient $df_{02}/dV_{g2}^{\rm DC} = 40\,$MHz/V. This number is orders of magnitude larger than those reported for other systems, such as 2 kHz/V for tunability with capacitive forces [35], 240 kHz/V with a Lorentz force [36], 40 kHz/V for piezoelectric NEMSs [37], and 10 kHz/V for a dielectric force setup [38]. Such a large frequency-shifting coefficient, as demonstrated by our CNT nanomechanical device, allows us to tune the phonon modes to be on-resonance or off-resonance with each other, offering a great ability to reconfigure the phonon-electron system to regions inaccessible in other systems.

C. Coupled resonators

Based on the fact that the resonators are highly tunable, we can study the electron-phonon strong coupling by varying the gate field [15, 16, 25, 27, 39]. Fixing $V_{g1}^{\rm DC} = -0.657$ V, and the corresponding resonance frequency $f_{01} = \omega_{m,1}/2\pi = 121.7$ MHz, we scan V_{g2}^{DC} to make f_{02} near-resonant with f_{01} and record the current I_{12}. In this case, we drive the two resonators simultaneously with two individual microwave sources at the same frequencies $f_{g1,2}$ (-43 dBm for resonator 1 and -49 dBm for resonator 2). To achieve a better resolution, we show the numerically-differentiated dI_{12}/df as a function of frequency $f_{g1,2}$ and $V_{g2}^{\rm DC}$ in Fig. 3(a). As indicated by the inclined arrow, f_{02} linearly decreases with increasing V_{g2}, and greatly modifies the current for the bias field that yields the peaks or dips observed in Fig. 2(c). At these points, we also observed a change of mechanical resonance frequency of $f_{0,2}$. Such phenomena arise from the strong phonon-electron tunneling interaction, which was firstly reported in 2009 [15, 16]. The fluctuation of electron charges on the CNT induces the back-action force on the mechanical modes, softening and damping the phonon modes [Fig. 3(c)]. The largest frequency shift is about 0.8 MHz, and the quality factors of the resonators are also largely reduced from 10,000 to 500 because of damping, corresponding to an increase of linewidth of phonon mode to 240 kHz. The frequency shift is about 3 times of magnitude larger than the linewidth of phonon mode, verifying the strong coupling of the mechanical motion and single-electron tunneling, and the damping rate induced by electron-phonon coupling $\gamma_{e-\rm ph}/2\pi \sim 240$ kHz, showing that the mechanical motion is largely damped at these points.

In contrast to previous results, obtained for single-nanotube mechanical oscillators, our system shows an additional vertical line (corresponding to resonator 1) where the frequency does not change with $V_{g2}^{\rm DC}$. This line clearly demonstrates the influence of resonator 2 on the electron charge in resonator 1, which provides evidence of the non-local control of the electron charge by phonons. When this line encounters the photon-electron tunneling interaction frequency, as shown in Fig. 3(b), the spectrum exhibits distinct features. A magnified 2D spectrum is shown in Fig. 4(a), with a clear avoided-crossing when scanning the frequency of resonator 2 by varying $V_{g2}^{\rm DC}$.

To quantitatively verify this phonon-phonon interaction mechanism, we also theoretically modeled the system using the Hamiltonian ($\hbar = 1$)

$$\mathcal{H}_m = \omega_{m,1} a_1^\dagger a_1 + \omega_{m,2} a_2^\dagger a_2 + \frac{\Omega}{2}(a_1^\dagger a_2 + a_1 a_2^\dagger), \quad (4)$$

where Ω is the phonon hopping between two resonators arising from the tunneling. Therefore, the coupling induced new normal modes with hybridization of two oscillators

$$A_\pm = \frac{1}{\mathcal{N}}[(\omega_\pm - \omega_{m,2})a_1 + \frac{\Omega}{2}a_2] \quad (5)$$

with normalization factor $\mathcal{N} = \sqrt{(\omega_\pm - \omega_{m,2})^2 + \frac{\Omega^2}{4}}$ and eigenfrequencies

$$\omega_\pm = \frac{1}{2}(\omega_{m,1} + \omega_{m,2} \pm \sqrt{(\omega_{m,1} - \omega_{m,2})^2 + \Omega^2}). \quad (6)$$

The calculated hybrid modes are shown in Fig. 4(b), by fitting the parameters from our system. The good correspondence with experiment confirms that the mechanism observed in Fig. 4(a) is coherent mechanical mode coupling. Especially, the obtained $\Omega/2\pi \approx 200$ kHz is an order of magnitude larger than $\kappa_{1,2}/2\pi \approx 10$ kHz. Therefore, the phonon-phonon coupling is in the strong-coupling regime $\Omega \gg \kappa_{1,2}$, and can be used for further coherent manipulation [40].

The coherent coupling is further studied for various V_{g1}. As indicated by Eq. 6, the coupling strength can be extracted directly through the minimum frequency difference between the hybrid modes ($\omega_{m,1} - \omega_{m,2} = 0$). Therefore, we plotted the spectrum of the minimum frequency splitting for different biased V_{g1}. Note that the V_{g1} changes the intrinsic frequency of $\omega_{m,1}$, thus the V_{g2} is adjusted to match the $\omega_{m,2}$ for each plot. Again, the two symmetrical dips in the spectrum confirm the equal

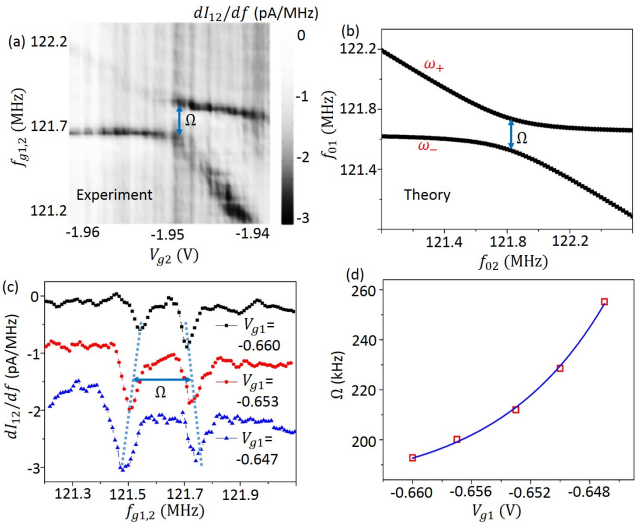

FIG. 4. **Strongly-coupled mechanical resonators** (a) Color map of the coupled resonators, where a clear avoided crossing of two resonance branches when the frequency of resonator 2 approaches the resonance frequency of resonator 1. The splitting frequency, Ω, represents the coupling strength of the system. (b) Theoretical calculation of the hybrid mechanical mode frequencies of the coupled resonators. (c) The spectrum of the current derivative as a function of the driving frequency for various gate voltages. (d) Coupling strength as a function of the gate voltage $V_{g1}^{\rm DC}$.

superposition of a_1 and a_2 (Eq. 5) for $\omega_{m,1} - \omega_{m,2} = 0$. Intriguingly, the coupling strength Ω shows a dependence on V_{g1}. This might be attributed to the increase of tension of the nanotubes with increasing V_{g1}, which reduces the evanescent phonon field on the S-electrode and suppresses the phonon tunneling. We find that the coupling strength Ω can be tuned from 190 kHz to 250 kHz when V_{g1} is varied from -0.66 V to -0.647 V (Fig. 4(d)).

D. Phononic quantum bus and discussion

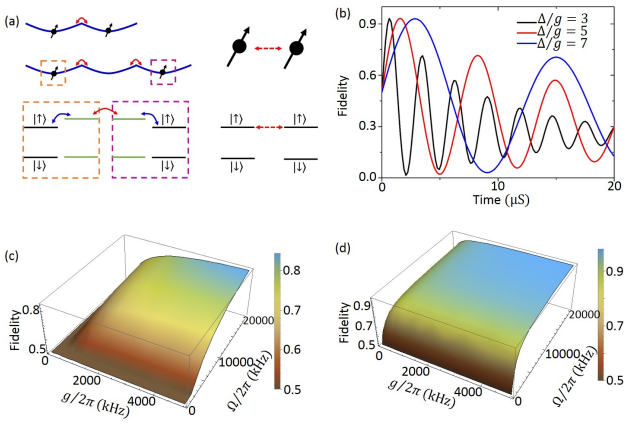

FIG. 5. **Phonon bus for spin qubits.** (a) Schematic diagram of the effective spin-spin interaction mediated by phonons, whose frequencies are largely detuned from the spin transition frequency. (b) Fidelity of the remote entangled spin state $|\psi\rangle = |\downarrow\uparrow\rangle - i\,|\uparrow\downarrow\rangle$ generation for different detunings, with $g/2\pi = 3000\,\mathrm{kHz}$, temperature $T = 30\,\mathrm{mK}$ and $\Omega = 5000\,\mathrm{kHz}$, and other parameters of mechanical resonators from our experiments. (c, d) show the fidelity versus spin-phonon coupling strength g and Ω, for $T = 300$ mK (c) and 30 mK (d).

Taking advantage of our novel fabrication method, the coupled CNT mechanical resonators could be extended to one dimensional resonator arrays, where a single CNT is put on a chip with multiple suspended sections. Combined with an electrically-configurable individual mode frequency and hopping rate, phonons could be manipulated and guided along the array on demand. Our study suggests that phonons are promising for quantum bus that can be used to transfer information over distances. It is instructive to consider two possible configurations: Given double quantum dots on each suspended section, phonons can assist single-electron tunneling between the dots, as demonstrated in Fig. 3. As a result, the quantum charge state can be coherently coupled with the localized phonon. Alternatively, according to the inherent curvature and the spin-orbit interaction [23, 24, 41], the spin states can be flipped by the phonons. Based on the phonon-phonon coupling demonstrated in this work, the excitation can be transferred between qubits over distance, and an effective qubit-qubit coupling can then be realized by the virtual collective phonon mode.

Specifically, we take the qubit as an example to illustrate the generation of spin entanglement states through the phononic quantum bus. As schematically shown in Fig. 5(a), there are two mechanical resonators each containing a single spin. More generally, such effects also hold for an array of resonators. For ideal conditions, without any dissipation or decoherence, the initial state $|\downarrow\uparrow\rangle$ of the system would evolve to the state $|\psi\rangle = |\downarrow\uparrow\rangle - i\,|\uparrow\downarrow\rangle$, which is the maximum entangled state over a distance of the order of microns. For practical parameters, spin-phonon coupling strength $g/2\pi = 3000\,\mathrm{kHz}$ [20, 21] (also see the supplementary materials), temperature $T = 30\,\mathrm{mK}$ and $\Omega = 5000\,\mathrm{kHz}$, the fidelity of the entanglement state $\mathcal{F} = \mathrm{Tr}[\rho(t)\,|\psi\rangle\,\langle\psi|)$ for various detuning Δ is plotted in Fig. 5(b) (see Methods for details). Owing to the trade-off between phonon relaxation γ_j and effective phonon-mediated coupling g_{eff}, a moderate detuning $\Delta/g = 7$ shows a longer coherence time and also maximum fidelity. In Fig. 5(c, d), the fidelity versus g and Ω is shown for $T = 300$ mK and 30 mK, respectively. The results indicate that both strong phonon-phonon coupling and spin-phonon coupling are important for remote-entanglement generation. Although the thermal-excitation decoherence substantially degrades the entanglement fidelity, it is still possible to observe this remote-entanglement effect in the current experiment setup ($T = 270$ mK) if we can increase the Ω to 10000 kHz by decreasing the width of S [Fig. 1(a)]. High-fidelity remote-entanglement generation ($\mathcal{F} > 0.95$) is promising with $T = 30$ mK, $g > 500$ kHz and $\Omega > 5000$ kHz, which are parameters that can be readily realized with current technologies.

In summary, we have studied the electron-phonon coupling in strongly-coupled carbon nanotube nanomechanical resonators. Our study suggests the use of phonons as coherent quantum information carriers to mediate the effective interaction between electron spins. The engineered phonons can also be used to initialize, readout and manipulate the electron spin states. Using phonons as flying qubits is the first step in the exploration of multiple degrees-of-freedom electron-phonon systems. Possible future works would investigate CNT mechanical resonator arrays in phononic quantum memories [42], also many-body interactions [43] and the implementation of possible quantum error correction schemes in coupled spin-phonon chains [44]. This system can even be further integrated with superconducting circuits to construct a hybrid quantum machine [45, 46].

METHODS

Sample preparation The CNTs were grown using the ethane CVD method on a silicon substrate with trenches. The prepared CNTs were all double- or triple-

walled CNTs, with diameters ranging from 2 to 3 nm. After depositing TiO2 nanoparticles onto the suspended parts of the CNTs for visualization, the inner shell of the CNTs were drawn out and placed in their proper positions with high precision using two homemade tips under an optical microscope. The electrodes and alignment marks were fabricated on an undoped silicon chip with 500 nm oxide, by optical lithography followed by metal deposition (5 nm Ti and 45 nm Au) with an electron-beam evaporator. Two gate electrodes beneath the resonators were fabricated by electron beam lithography (EBL) followed by metal deposition (5 nm Ti and 45 nm Au). Finally, the contact electrodes (10 nm Ti and 190 nm Au) were fabricated, to decrease the residual resists as much as possible. The EBL resists used here were single-layered PMMA 950 A4 for the gates and double-layered for the contacts. After the transfer process, electrical annealing was used to improve the contact. The resistance of our devices was typically several hundred kΩ at room temperature.

Detection The driving AC signals were produced by two individual analogue signal generators (Agilent E8257D), attenuated by 30 dB at room temperature, then transmitted to the sample through Lake-Shore cables. There was an approximately 5 dB attenuation in the cable; however, we estimate a ∼3 dB error from sample to sample in our setup. Gate and bias DC voltages are controlled by the DC ports of a lock-in amplifier (SR830). AC and DC voltages are combined by a bias-T (Anritsu K251). Current through the resonator was measured by a multi-meter, after a pre-amplifier (SR570).

Theory of phonon mediated entanglement Considering the simple two-resonator case studied here, we obtain the system Hamiltonian as [20–22]

$$\mathcal{H} = \mathcal{H}_m + \frac{1}{2}(\omega_{s,1}\sigma_{z,1} + \omega_{s,2}\sigma_{z,2}) + g(\sigma_{1,-}a_1^\dagger + \sigma_{2,-}a_2^\dagger + \sigma_{1,+}a_1 + \sigma_{2,+}a_2). \quad (7)$$

For simplicity, we assume the phonon modes and spins are identical ($\omega_{s,1} = \omega_{s,2}$ and $\omega_{m,1} = \omega_{m,2}$). In the normal mode representation, we have $A_\pm = \frac{1}{\sqrt{2}}(a_1 \pm a_2)$, whose frequencies differ by Ω. Allowing the phonon modes to be largely detuned from the spin transitions ($\omega_{s,1} = \omega_{m,1} - \Omega/2 - \Delta$), therefore mediates the spin-spin interaction but rarely absorb the excitations. By adiabatic elimination of the phonon modes, the spins obey the Master equation as $\frac{d}{dt}\rho = -i[\mathcal{H}_{eff}, \rho] + \sum_{j=1,2}[\frac{\gamma_{j,ph}}{4}\mathcal{L}(\sigma_{j,z}, \rho) + \frac{\gamma_j}{2}(n_{th}+1)\mathcal{L}(\sigma_{j,-}, \rho) + \frac{\gamma_j}{2}n_{th}\mathcal{L}(\sigma_{j,+}, \rho)]$, where the effective Hamiltonian is

$$\mathcal{H}_{eff} = g_{eff}(\sigma_{1,-}\sigma_{2,+} + \sigma_{1,+}\sigma_{2,-}), \quad (8)$$

with $g_{eff} \approx \frac{g^2\Omega/2}{\Delta(\Delta+\Omega)}$ and Lindbald form $\mathcal{L}(o, \rho) = 2o\rho o^\dagger - o^\dagger o\rho - \rho o^\dagger o$. Here, the pure dephasing rate $\gamma_{j,ph}/2\pi = 1\,\text{kHz}$ is estimated from hyperfine interaction [47], and the intrinsic energy relaxation is neglected owing to the negligible environment phonon density of state, and the effective energy relaxation rate arising from $a_{1,2}$ is $\gamma_j \approx \frac{g^2\kappa(\Delta^2+\Delta\Omega+\Omega^2/2)}{\Delta^2(\Delta+\Omega)^2}$.

[1] Saito, R., Dresselhaus, G., and Dresselhaus, M. S. *Physical Properties of Carbon Nanotubes.* World Scientific Publishing, (1998). ISBN 978-1-86094-093-4 (hb) ISBN 978-1-86094-223-5 (pb).

[2] Ilani, S. and McEuen, P. L. *Annu. Rev. Condens. Matter Phys.* **1**(1), 1–25 (2010).

[3] Laird, E. A., Kuemmeth, F., Steele, G. A., Grove-Rasmussen, K., Nygard, J., Flensberg, K., and Kouwenhoven, L. P. *Reviews Of Modern Physics* **87**(3), 703–764 (2015).

[4] Biercuk, M. J., Garaj, S., Mason, N., Chow, J. M., and Marcus, C. M. *Nano Lett.* **5**(7), 1267–1271 (2005).

[5] Sapmaz, S., Meyer, C., Beliczynski, P., Jarillo-Herrero, P., and Kouwenhoven, L. P. *Nano Lett.* **6**(7), 1350–1355 (2006).

[6] Sapmaz, S., Jarillo-Herrero, P., Kouwenhoven, L. P., and Zant, H. S. J. V. D. *Semicond. Sci. Technol.* **21**(11), S52–S63 (2006).

[7] Grove-Rasmussen, K., Jø rgensen, H. I., Hayashi, T., Lindelof, P. E., and Fujisawa, T. *Nano Lett.* **8**(4), 1055–1060 (2008).

[8] Jung, M., Schindele, J., Nau, S., Weiss, M., Baumgartner, A., and Schönenberger, C. *Nano Lett.* **13**(9), 4522–4526 (2013).

[9] Petersson, K. D., McFaul, L. W., Schroer, M. D., Jung, M., Taylor, J. M., Houck, a. a., and Petta, J. R. *Nature* **490**(7420), 380–383 (2012).

[10] Deng, G. W., Wei, D., Li, S. X., Johansson, J. R., Kong, W. C., Li, H. O., Cao, G., Xiao, M., Guo, G. C., Nori, F., Jiang, H. W., and Guo, G. P. *Nano Lett.* **15**(10), 6620–6625 (2015).

[11] Meunier, T. and Ba, C. *Nature* **477**(7365), 435–438 (2011).

[12] Mcneil, R. P. G., Kataoka, M., Ford, C. J. B., Barnes, C. H. W., Anderson, D., Jones, G. A. C., Farrer, I., and Ritchie, D. A. *Nature* **477**(7365), 439–442 (2011).

[13] Laird, E. A., Pei, F., Tang, W., Steele, G. A., and Kouwenhoven, L. P. *Nano Lett.* **12**(1), 193–197 (2012).

[14] Moser, J., Eichler, A., Guttinger, J., Dykman, M. I., and Bachtold, A. *Nat. Nanotechnol.* **9**(12), 1007–1011 (2014).

[15] Steele, G. A., Huttel, A. K., Witkamp, B., Poot, M., Meerwaldt, H. B., Kouwenhoven, L. P., and Zant, H. S. J. v. d. *Science* **325**(5944), 1103 (2009).

[16] Benjamin, L., Yury, T., Jari, K., David, G.-S., and Adrain, B. *Science* **325**, 1107 (2009).

[17] Ando, T. *J. Phys. Soc. Japan* **69**(6), 1757–1763 June (2000).

[18] Huertas-Hernando, D., Guinea, F., and Brataas, A. *Phys. Rev. B* **74**(15), 155426 (2006).

[19] Kuemmeth, F., Ilani, S., Ralph, D. C., and McEuen, P. L. *Nature* **452**(7186), 448–452 (2008).

[20] Palyi, A., Struck, P. R., Rudner, M., Flensberg, K., and

Burkard, G. *Phys. Rev. Lett.* **108**(20), 206811 (2012).
[21] Ohm, C., Stampfer, C., Splettstoesser, J., and Wegewijs, M. R. *Appl. Phys. Lett.* **100**(14), 143103 (2012).
[22] Wang, H. and Burkard, G. *Phys. Rev. B* **90**(3), 035415 July (2014).
[23] Bulaev, D. V., Trauzettel, B., and Loss, D. *Phys. Rev. B* **77**(23), 235301 (2008).
[24] Rudner, M. S. and Rashba, E. I. *Phys. Rev. B* **81**(12), 125426 (2010).
[25] Benyamini, a., Hamo, A., Kusminskiy, S. V., von Oppen, F., and Ilani, S. *Nat. Phys.* **10**(2), 151–156 January (2014).
[26] Zippilli, S., Morigi, G., and Bachtold, A. *Phys. Rev. Lett.* **102**(9), 096804 mar (2009).
[27] Meerwaldt, H. B., Labadze, G., Schneider, B. H., Taspinar, A., Blanter, Y. M., van der Zant, H. S. J., and Steele, G. A. *Phys. Rev. B* **86**(11), 115454 (2012).
[28] Wang, H. and Burkard, G. *Phys. Rev. B* **92**(19), 195432 nov (2015).
[29] Rabl, P., Kolkowitz, S. J., Koppens, F. H. L., Harris, J. G. E., Zoller, P., and Lukin, M. D. *Nat. Phys.* **6**(8), 602–608 May (2010).
[30] Gustafsson, M. V., Aref, T., Kockum, A. F., Ekstrom, M. K., Johansson, G., and Delsing, P. *Science* **346**(6206), 207–211 September (2014).
[31] Schuetz, M. J. a., Kessler, E. M., Giedke, G., Vandersypen, L. M. K., Lukin, M. D., and Cirac, J. I. *Phys. Rev. X* **5**(3), 031031 (2015).
[32] Liang, W., Bockrath, M., Bozovic, D., Hafner, J. H., Tinkham, M., and Park, H. *Nature* **411**(6838), 665–669 (2001).
[33] Grove-Rasmussen, K., Jø rgensen, H. I., and Lindelof, P. E. *Phys. E Low-Dimensional Syst. Nanostructures* **40**(1), 92–98 (2007).
[34] Huttel, A. K., Steele, G. a., Witkamp, B., Poot, M., Kouwenhoven, L. P., and Van Der Zant, H. S. J. *Nano Lett.* **9**(7), 2547–2552 (2009).
[35] Rugar, D. and Grutter, P. *Phys. Rev. Lett.* **67**(6), 699–702 (1991).
[36] Karabalin, R. B., Cross, M. C., and Roukes, M. L. *Phys. Rev. B* **79**(16), 165309 apr (2009).
[37] Mahboob, I. and Yamaguchi, H. *Nature Nanotech.* **3**(5), 275–279 (2008).
[38] Unterreithmeier, Q. P., Weig, E. M., and Kotthaus, J. P. *Nature* **458**(7241), 1001–1004 (2009).
[39] Moser, J., Guttinger, J., Eichler, A., Esplandiu, M. J., Liu, D. E., Dykman, M. I., and Bachtold, A. *Nature Nanotech.* **8**, 493 (2013).
[40] Faust, T., Rieger, J., Seitner, M. J., Kotthaus, J. P., and Weig, E. M. *Nature Phys.* **9**(8), 485–488 (2013).
[41] Steele, G. A., Pei, F., Laird, E. A., Jol, J. M., Meerwaldt, H. B., and Kouwenhoven, L. P. *Nat. Commun.* **4**, 1573 (2013).
[42] Zhang, X., Zou, C.-L., Zhu, N., Marquardt, F., Jiang, L., and Tang, H. X. *Nat. Commun.* **6**, 8914 nov (2015).
[43] Soykal, O. O. and Tahan, C. *Phys. Rev. B* **88**(13), 134511 October (2013).
[44] Waldherr, G., Wang, Y., Zaiser, S., Jamali, M., Schulte-Herbrüggen, T., Abe, H., Ohshima, T., Isoya, J., Du, J. F., Neumann, P., and Wrachtrup, J. *Nature* **506**(7487), 204–7 February (2014).
[45] Xiang, Z.-L., Ashhab, S., You, J., and Nori, F. *Rev. Mod. Phys.* **85**(2), 623–653 apr (2013).
[46] Deng, G.-W., Wei, D., Johansson, J. R., Zhang, M.-L., Li, S.-X., Li, H.-O., Cao, G., Xiao, M., Tu, T., Guo, G.-C., Jiang, H.-W., Nori, F., and Guo, G.-P. *Phys. Rev. Lett.* **115**(12), 126804 sep (2015).
[47] Csiszar, G. and Palyi, A. *Phys. Rev. B* **90**(24), 245413 (2014).

ACKNOWLEDGMENT

We thank Liang Jiang, Lin Tian and Guido Burkard for beneficial discussions. This work was supported by the National Fundamental Research Program (Grant No. 2011CBA00200), the Strategic Priority Research Program of the Chinese Academy of Sciences (Grant No. XDB01030000), and the National Natural Science Foundation (Grants No. 11222438, 11174267, 61306150, 11304301, and 91421303). This work was also supported by the National Basic Research Program of China (2012CB932301), National Key Basic Research Program of China (MOST 2013CB922003) and NSF of China (No. 11474178).

AUTHOR CONTRIBUTION

G.W.D. and D.Z. conceived the device. D.Z., X.H.W., K.L.J., D.L. and Y.L. fabricated the samples. G.W.D., H.O.L., G.C., G.C.G. and M.X. performed the measurements. G.W.D., D.Z. and X.H.W. analyzed the data. C.L.Z. and G.P.G. conducted the theoretical investigation. G.P.G. supervised the project. All authors contributed to the writing of this paper.

ADDITIONAL INFORMATION

Competing financial interest: The authors declare that they have no competing financial interests.